Metal artifact reduction for intracranial projectiles on post mortem computed tomography

N. Douis, A.S. S Formery, G. Hossu, L. Martrille, M. Kolopp, P.A. A Gondim Teixeira, A. Blum

Diagnostic and Interventional Imaging (2020) **101**, 177—185

ORIGINAL ARTICLE /*Forensic medicine*

Metal artifact reduction for intracranial projectiles on post mortem computed tomography

N. Douis[a,*], **A.S. Formery**[b], **G. Hossu**[e], **L. Martrille**[c], **M. Kolopp**[d], **P.A. Gondim Teixeira**[a], **A. Blum**[a]

[a] *Guilloz Imaging Department, Hopital Central, CHU Nancy, 54000 Nancy, France*
[b] *Claude Bernard Clinic, 57070 Metz, France*
[c] *Forensic Institute, Hospitaux de Brabois, CHU Nancy, 54500 Nancy, France*
[d] *Forensic Institute, Hopital La Timone, AP-HM, 13005 Marseille, France*
[e] *Lorraine University, Inserm, IADI, 54000 Nancy, France*

KEYWORDS
Autopsy;
Computed tomography (CT);
Cadaver;
Gunshot wounds;
Artifacts

Abstract
Purpose: To compare the image quality of cranial post-mortem computed tomography (CT) obtained with and without projection-based single-energy metal artifact reduction (SEMAR) in cadavers with intracranial metallic ballistic projectiles.
Materials and methods: From January 2017 to January 2018, cadavers with ballistic projectile head wounds with metal fragments and without massive head destruction were investigated using post-mortem CT. All subjects underwent CT using a conventional iterative reconstruction (IR) and SEMAR. To evaluate the impact of metallic artifacts, the total intracranial area (TA), non-interpretable zone (NIZ), disturbed interpretation zone (DZ), and artifact total surface (ATS) were delineated. Two independent readers identified extra-axial hemorrhage (EAH) and subarachnoid hemorrhage (SAH). Autopsy reports were used as the standard of reference.
Results: Eleven corpses (10 males, 1 female; mean age, 62.8 ± 17.9 [SD] years) were evaluated. SEMAR showed a significant decrease in the ATS ratio with respect to conventional IR (72.1 ± 26.1 [SD] % [range: 26.8-99.1] vs. 86.4 ± 17.8 [SD] % [range: 37.2-100]; $P < 0.001$) and NIZ/TA ratios (11.6 ± 8.26% [range: 0.95—33.4] versus 42.5 ± 30.5% [range: 3.86—100]; $P < 0.001$). The inter-observer reproducibility in diagnosing EAH and SAH was excellent with conventional IR (0.82) and good with SEMAR (0.75). SEMAR reduced uncertain diagnoses of EAH in 7 subjects for Reader 1 and in 6 for Reader 2, but did not influence the diagnosis of SAH for either reader.
Conclusion: SEMAR reduces the influence of metallic artifacts and increases the confidence with which the diagnosis of EAH can be made on post-mortem CT.

* Corresponding author.
E-mail address: douisnicolas@gmail.com (N. Douis).

https://doi.org/10.1016/j.diii.2019.10.009

Performing unenhanced post-mortem computed tomography (PMCT) has become a common practice during the forensic evaluation of deceased subjects [1—3]. PMCT allows subject evaluation with no compromise to body integrity and is particularly effective at detecting bone fractures and foreign objects, which are crucial aspects of the forensic investigation. Regarding ballistic head trauma, various studies have demonstrated that analysis of native CT images, multiplanar reconstructions, and three dimensional (3D) volume-rendered reconstructions could guide and increase the accuracy of autopsies [4—13]. Although entry and exit bullet wounds are best evaluated by direct examination, PMCT can assist in the recovery of bullets and bullet fragments and provides a detailed evaluation of all bony structures, some of which are difficult to access at autopsy [14—20].

Although the exact prevalence is unknown, the presence of retained metal fragments in the head following gunshot wounds is frequent. Metallic foreign bodies are an important source of artifact on CT, hampering or even precluding image interpretation. Metallic artifacts are caused mainly by beam hardening, photon starvation, and edge profile errors [21,22]. Metallic artifacts are particularly problematic, as bullets comprised of metals and metal alloys with high atomic numbers are responsible of considerable CT image degradation.

Various CT image reconstruction algorithms designed to reduce metal artifacts are available and help improve image quality in the presence of metallic prostheses in different body areas [23—29]. As firearm projectiles have a different composition than prosthetic implants, the performance of these algorithms to evaluate gunshot wounds is uncertain. An animal study showed the potential of metal artifact reduction techniques (iMAR) for the assessment of retained bullets in the head with CT [30]. Among the techniques available for metal artifact reduction on CT, single-energy metal artifact reduction (SEMAR, Canon Medical Systems) with raw data interpolation has been studied in patients with considerable improvements in image quality [31,32]. We hypothesized that SEMAR could increase the image quality of PMCT images in head gunshot wound victims, improving the analysis of cranial hemorrhagic lesions.

The purpose of this study was to compare the image quality of PMCT obtained with and without SEMAR in cadavers with intracranial metallic ballistic projectiles.

Material and methods

Subjects

From January 2017 to January 2018, 126 subjects underwent PMCT in our institution, requested by a magistrate as part of the conventional judicial procedure. Subject age, sex, and cause of death were evaluated. Among these subjects, there were 29 gunshot wounds, 21 of which were located in the head. The exclusion criteria were: unanalyzable cerebral parenchyma (putrefaction, head destruction), absence of metallic projectile fragments in the head or impossibility to select the CT images containing a single metallic body, and absence of iterative reconstruction with SEMAR. Five subjects with no retained metallic fragments in the head and five subjects with available SEMAR reconstruction were excluded. Thus, the final study population was composed of 11 cadavers (10 males and 1 female), with a mean age of 62.8 ± 17.9 (standard deviation [SD] years) (range: 40—93 years). Fig. 1 shows subjects inclusion into the study. The cause of death in all included subjects was suicide by gunshot wound to the head. In our institution, ethics committee approval is not required for retrospective, anonymized studies based on deceased subjects requested as part of a judicial procedure.

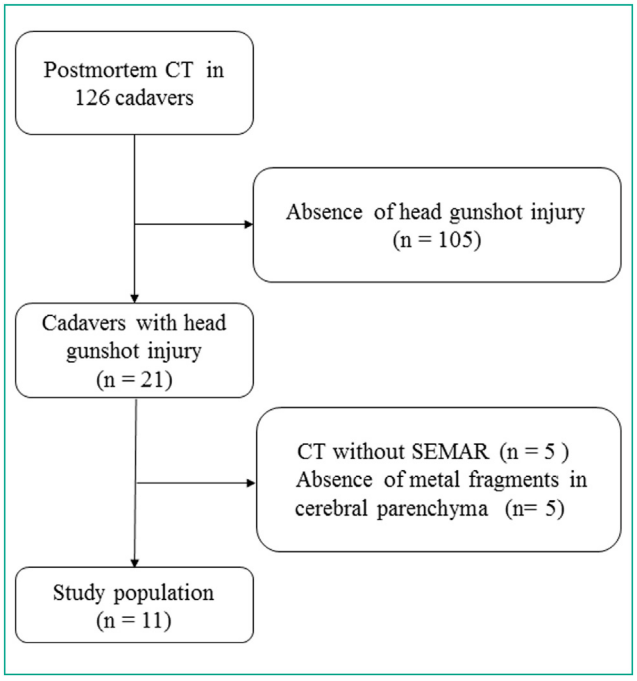

Figure 1. Flow chart diagram of included and excluded cadavers.

Acquisition protocol

CT images were acquired with a 320 detector-row CT scanner (Aquilion® One, Canon Medical Systems). A whole-body acquisition was performed in all subjects. The acquisition parameters for head imaging were: 0.75s tube rotation time, 135 kVp, 450 mA, 0.5 mm slice thickness, FOV 24 cm, and matrix 512 × 512; for one subject, slice thickness was 1 mm. A standard head reconstruction kernel (FC26) was used for all reconstructions. For each study, two volumes of the head were reconstructed, one using an adaptive IR algorithm (AIDR 3D, Canon Medical Systems) herein named as conventional IR and another with SEMAR.

Image analysis

CT image quality was assessed by a radiologist (N.D) with two years of medical imaging experience. Original CT images of the brain in the axial plane were browsed to select images containing a single metallic fragment in order to avoid the combined effect of multiple fragments on image quality. For five subjects, more than one image showing a single metallic body was available. These images were evaluated independently. The same images were used for analysis with conventional IR and SEMAR reconstructions.

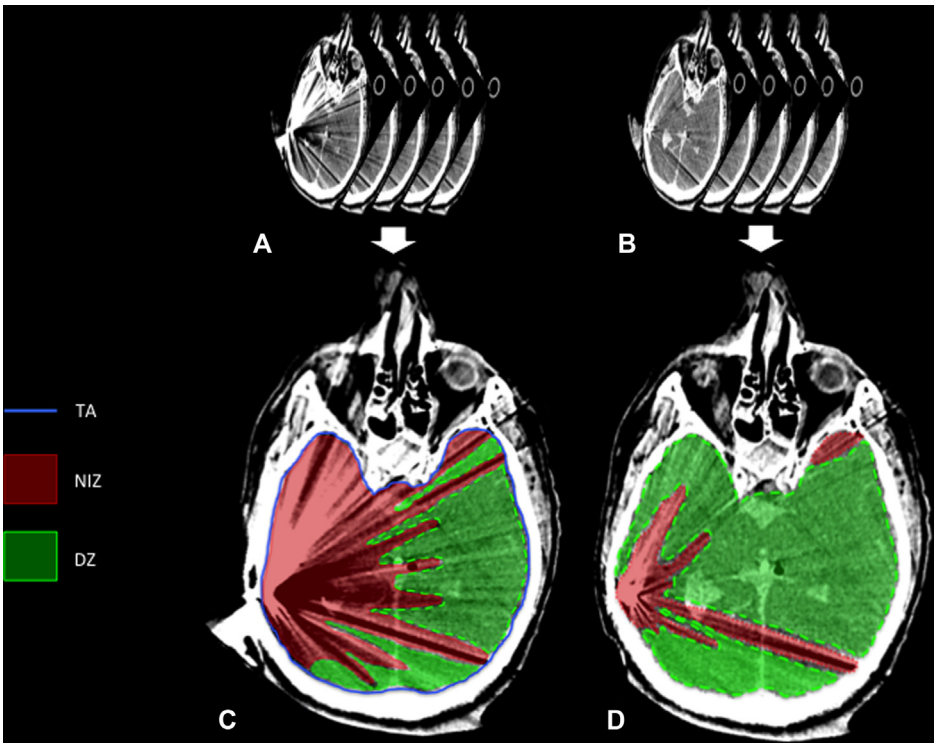

Figure 2. Description of region of interest placement on CT images in a 47-year-old male cadaver. Head CT images reconstructed with conventional iterative reconstruction (A) and with single-energy metal artifact reduction (SEMAR) (B) were browsed to select an axial image showing a single metallic foreign body (C and D). A metallic projectile fragment located adjacent to the inner surface of the temporal bone (arrow) generating important metallic artifacts. The total cranial area is delineated by a continuous blue line, the red area represents the zone that is non-interpretable zone, and the green area represents the zone disturbed by metal artifacts. Note that in D the non-interpretable zone is much smaller than in C.

The maximum diameter of the target metallic fragments was measured on conventional IR using a wide window setting (C1000/W9000 HU). The influence of metallic artifacts in the evaluation of cranial hemorrhagic lesions was evaluated using a 40/80 HU window setting with both conventional IR and SEMAR CT images using the following procedure (Fig. 2). A first freeform region of interest (ROI) was used to delineate the total intra-cranial area in mm^2 in the selected slices (TA). A second freeform ROI was used to delineate the area in mm^2 completely obscured by metallic artifacts (non-interpretable zone—NIZ). A third freeform ROI was used to delineate the area in mm^2 in which metallic artifacts were present, but CT image analysis was still possible (disturbed zone—DZ). Artifact total surface (ATS) was calculated using the following equation: ATS = (NIZ + DZ). NIZ/TA, DZ/TA, and ATS/TA ratio were calculated for each metal fragment evaluated and for subjects considering all fragments evaluated in each subject.

Diagnostic performance for cerebral hemorrhage was evaluated by analyzing all CT images reconstructed with and without SEMAR. Two radiologists, with 2- and 7-years of medical imaging experience respectively, independently evaluated PMCT images for the detection of extra-axial hemorrhage (EAH), including epidural hematoma (EDH) and acute subdural hematoma (ASDH), as well as subarachnoid hemorrhage (SAH). An EDH was diagnosed when a spontaneously hyperattenuating elliptical lesion was observed between the cranial vault and when cerebral parenchyma was identified. An ASDH was diagnosed when a crescent-shaped spontaneously hyperattenuating CT image was observed at the location of the subdural space. SAH was diagnosed when the subarachnoid space and cisterns were spontaneously hyperattenuating [33]. The diagnostic confidence for hemorrhagic lesions was graded using a Likert scale (1 = definitely absent; 2 = likely absent; 3 = uncertain; 4 = definitely present; and 5= not analyzable).

The location of the entry and exit wounds was evaluated on images with and without SEMAR and correlated with autopsy findings.

Standard of reference

An autopsy was performed using a standardized technique for all included cadavers. First, the body was externally examined. A coronal scalp incision from one retro-auricular region to the other was then performed, followed by receding of the scalp forward and backward. The cranial vault was opened using an electric saw. Photographs of autopsy findings were available for all subjects except one. Autopsy reports and photographs were reviewed retrospectively by a forensic physician with 4 years of clinical experience to standardize the description and nomenclature of cranial lesions. For the autopsy with no photographs available, the initial autopsy report was used because the description was deemed sufficiently clear, using a similar lesion nomenclature.

Statistical analysis

Statistical analysis was performed using R Development Core Team software (version 3.2.0 2015). Quantitative data were presented as mean ± SD (range: minimum—maximum in %). Ratios between NIZ, DZ, and ATS with respect to TA were used to allow inter-subject data comparison. As some subjects presented multiple metallic fragments, these data were presented in a per-fragment and per -subject basis. A paired Wilcoxon test was used to compare the sizes of the zones measured with conventional IR and SEMAR. A *P* value less than 0.05 was considered to indicate statistical significance. Kappa test was used to evaluate interobserver reproducibility for the diagnosis of intracranial hemorrhagic lesions. Kappa values of 0.00-0.20 were considered to indicate poor agreement; 0.21-0.4, fair; 0.41-0.60, moderate; 0.61-0.80, good and 0.81-1, excellent agreement. Autopsy reports were used as the standard of reference for the evaluation of intracranial hemorrhagic lesions and Fisher exact test was used to evaluate diagnostic accuracy.

Results

Among the 11 cadavers, 20 CT images with artifacts arising from a single metallic foreign body were identified (mean of 1.8 ± 1.1[SD] images per CT study [range: 1-4]). The mean metallic fragment maximum diameters were 5.9 ± 2.5 [SD] mm (range: 3.15-12.05 mm).

For all subjects, no additional elements contradicting death by suicide were found after autopsy. The used weapon and ammunition caliber varied. The rifle models used were: three carbines 5.56 × 15 mm R (22 long rifle), one automatic with unknown caliber, one hunting rifle with unknown caliber, two single shot rifles with a 12 mm caliber. Three handguns were also used: one automatic pistol 6.35 mm (.25 Automatic Colt Pistol, one single shot pistols 5.56 × 15 mm R (22 long rifle) and one revolver 9 mm (0.38 special wadcutter). There was also a modified single shot pistol 5.56 × 15 mm R (22 long rifle) caliber. The used ammunition type was unknown.

A significant decrease in mean ATS ratios per fragment was found with SEMAR (72.1 ± 26.1 [SD] % [range: 26.8-99.05%]) compared to conventional IR (86.4 ± 17.8 [SD] % [range: 37.2-100%]) (*P* < 0.001). A similar variation was found with ATS ratios per subject with and without SEMAR (75.41 ± 21.69 [SD] % [range: 39.95—98.28%] and 87.94 ± 19.13 [SD] % [range: 37.22-100], respectively). A significant decrease mean NIZ ratio was found with SEMAR compared to conventional IR (*P* < 0.001). The mean NIZ ratio with and without SEMAR per fragment was 11.6 ± 8.26 [SD] % (range: 0.95—33.39%) and 42.5 ± 30.5 [SD] % (range: 3.86—100%), respectively, and per subject was 13.15 ± 9.43 [SD] % (range: 0.95—33.39%) and 52.66 ± 31.40% (range: 3.86-100%), respectively. No significant difference in DZ ratios per fragment between conventional IR and SEMAR CT images was observed (*P* = 0.07). A relative increase in mean DZ ratios per fragment with SEMAR with respect to conventional IR was observed (mean DZ ratio with and without SEMAR 60.4 ± 24.4 [SD] % [range: 13.9-92.5%] and 43.7 ± [SD] 24% [range: 0-75.64%], respectively) (Table 1). DZ ratios per subject varied with and without SEMAR (62.29 ± 20.88 [SD] % [range: 39—89.22%] and 35.01 ± 21.0 [SD] % [range: 0—63.07%], respectively).

The interobserver variability for the diagnosis of EAH and SAH was excellent with conventional IR (Kappa = 0.82, IC 95%[0.99-0.64]) and good with SEMAR (Kappa = 0.75, IC 95%[0.96-0.54]) [34]. In two subjects, the evaluation of intracranial hemorrhagic lesions was not feasible both on imaging and on autopsy due to head destruction.

A total of 13 hemorrhagic cranial lesions were deemed present at autopsy, including SAH in eight subjects and EAH in five subjects. If grade 1 was considered as a negative diagnosis and grade 4 as a positive diagnosis, ten of these lesions were correctly diagnosed by both readers with conventional IR and SEMAR. For both readers, 100% (8/8) of the SAH were correctly diagnosed while only 40% (2/5) of the EAH were correctly diagnosed. Regarding diagnostic confidence, the number of uncertain diagnoses decreased with SEMAR for both readers. In five and four subjects respectively for Readers 1 and 2, the diagnostic confidence for EAH changed from uncertain with conventional IR to likely absent with SEMAR, and in two lesions for both readers, the diagnostic confidence for EAH changed from likely absent to definitely absent (Fig. 3). In all these subjects, an autopsy confirmed the absence of these lesions. When SEMAR was compared to IR, a significant increase in the diagnostic accuracy of ASDH was found for Reader 1 (*P*=0.012). No significant diagnostic accuracy differences were found for EDH (*P* = 0.175) for this reader. For Reader 2, the differences in diagnostic accuracy for EAH between SEMAR and IR were not statistically significant (*P* = 0.0615 and *P* = 0.175, respectively for EDH and ASDH).

With both SEMAR and conventional IR, there were two false-positive diagnoses of EAH for Reader 1 and three for Reader 2, as well as one false-negative diagnosis of EAH for each reader (Fig. 4). Moreover, with SEMAR CT images, there was one additional EAH false-positive diagnosis for each reader and one EAH false negative for Reader 2.

The location of the entry and exit wound was correctly identified in all cases with both SEMAR and conventional IR images.

Discussion

A significant reduction in metal artifact influence on PMCT with SEMAR was observed compared with conventional IR, with a significant decrease in both ATS and NIZ ratios per fragment. A similar variation was seen with ATS and NIZ ratios per patient. These results are in accordance with previous literature reports on CT metal artifact reduction in live patients [23,24,26,31,35—37]. In addition, SEMAR significantly increased the diagnostic accuracy for aSDH compared to IR for reader 1. However, there were no significant changes in accuracy for reader 2 nor for the diagnosis of EDH for reader 1, which might be explained by the small sample size. The diagnostic confidence in cranial hemorrhagic lesion identification increased with a lower number of uncertain diagnosis for both readers with SEMAR. The interobserver variability, however, was slightly worse with SEMAR, which is likely related to the decrease in the number of uncertain diagnoses. Although SAH was correctly identified in all subjects with both algorithms, the number of

Table 1 Metal artifact measures without and with SEMAR and calculation of NIZ, DZ, and ATS ratios.

Subject	IS	T fm (mm)	TA (mm^2)	NIZ (mm^2)	NIZ/TA (%)	DZ (mm^2)	DZ/TA (%)	ATS/TA (%)	NIZ (mm^2)	NIZ/TA (%)	DZ (mm^2)	DZ/TA (%)	ATS/TA (%)
1	1	7.72	12255.01	9552.62	77.94	2269.75	18.52	96.47	793.85	6.48	9967.89	81.34	87.82
2	2	6.25	2448.08	1992	81.37	317.8	12.98	94.35	631.51	25.80	959.67	39.20	65.00
3	3	9.24	11564.23	5230.74	45.23	5962.82	51.56	96.79	1489.85	12.88	1612.94	13.95	26.83
3	4	8.66	9647.06	9647.06	100	0.00	0.00	100	1675.48	17.37	7396.05	76.67	94.03
4	5	3.03	15383.92	963.19	6.26	10736.91	69.79	76.05	242.40	1.58	4285.25	27.86	29.43
4	6	8.07	11328.69	5740.40	50.67	4240.38	37.43	88.10	1433.08	12.65	8160.40	72.03	84.68
4	7	3.61	9393.99	969.35	10.32	4499.30	47.90	58.21	192.94	2.05	2493.11	26.54	28.59
5	8	8.82	7943.68	5950.94	74.91	1992.74	25.09	100.00	2652.55	33.39	4502.71	56.68	90.07
6	9	4.69	8631.10	3344.54	38.74	5038.38	58.37	97.12	1421.59	16.47	6073.27	70.36	86.84
6	10	6.48	8385.72	2722.58	33.92	5303.14	63.24	100.00	1393.20	16.61	6621.83	78.97	95.58
7	11	4.21	13311.42	1519.68	11.41	9419.77	70.76	82.18	925.59	6.95	6539.18	49.12	56.08
7	12	4.54	11522.6	2347.98	20.37	8715.71	75.64	96.02	1409.73	12.23	5992.23	52.00	64.24
7	13	3.54	8292	2619.41	31.59	1952.10	23.54	53.56	1447.74	17.46	2830.47	34.13	51.59
7	14	3.15	7779.99	960.87	12.35	4691.02	60.30	72.65	227.52	2.92	4127.30	53.05	55.97
8	15	4.23	9853.87	3024.87	30.70	5977.60	60.66	91.36	382.98	3.89	9119.52	92.55	96.43
8	16	4.93	10154.67	3292.56	32.42	6069.10	59.77	92.19	993.16	9.78	8770.5	86.37	96.15
8	17	4.89	8534.53	2506.5	29.36	5870.92	68.79	98.16	880.22	10.31	7573.31	88.74	99.05
9	18	1.95	9439.81	364.41	3.86	3149.09	33.36	37.22	89.96	0.95	3681.42	39.00	39.95
10	19	8.8	8079.12	8079.12	100	0.00	0.00	100.00	1107.46	13.71	6569.30	81.31	95.02
11	20	10.5	11820.06	7207.36	60.97	4296.41	36.35	100.00	1114.47	9.43	10502.42	88.85	98.28
mean ± SD	5.86 ± 2.49	9788.48 ± 2658.25	3901.81 ± 2894	42.55 ± 30.52	4525.147 ± 2975.12	43.70 ± 23.96	86.38 ± 17.78	1025 ± 630.63	11.64 ± 8.26	5888.94 ± 2756.19	60.44 ± 24.35	72.08 ± 26.09	
[range]	[1.95—10.5]	[2448.08—15383.92]	[364.41—9552.62]	[3.86—100]	[0—109419.7]	[0—75.64]	[37.22—100]	[89.96—2652.55]	[0.95—33.39]	[959.67—10502.42]	[13.9—92.5]	[26.82—99.05]	

IS: Selected images; T fm: Metal fragment size; TA: Total intracranial area; NIZ: Non-interpretable zone; DZ: Disturbed interpretation zone; ATS: Artifact total surface; IR: Conventional iterative reconstruction; SEMAR: Single-energy metal artifact reduction.

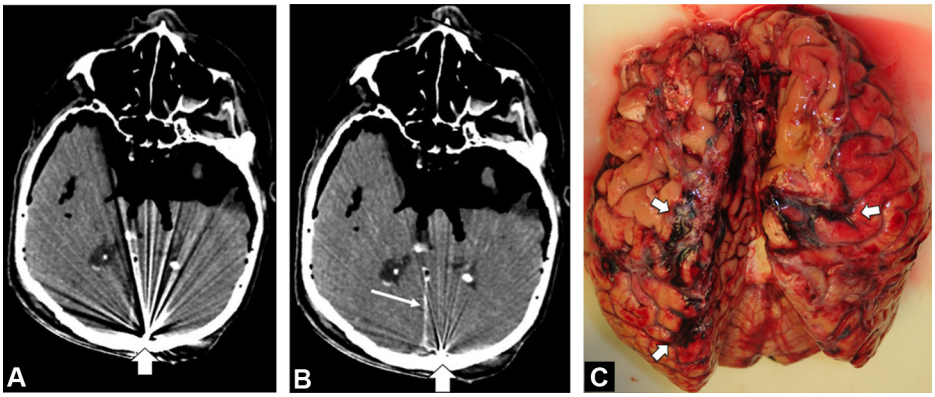

Figure 3. A 67-year-old man victim of a head gunshot would. A, CT image in the axial plane obtained with conventional iterative reconstruction at the level of temporo-occipital lobes with metallic projectile against inner occipital bone (large arrow) generating artifacts, which hamper the analysis of the cerebral parenchyma. B) Axial computerized tomography image reconstructed with single-energy metal artifact reduction (SEMAR) at the same location shows marked reduction in metallic artifacts enabling better analysis of cerebral parenchyma and meninges. Spontaneous hyperattenuating area of the falx (thin arrow) indicative of subarachnoid hemorrhage (SAH) can be seen. C) Photograph obtained during autopsy confirms various foci of SAH (arrows).

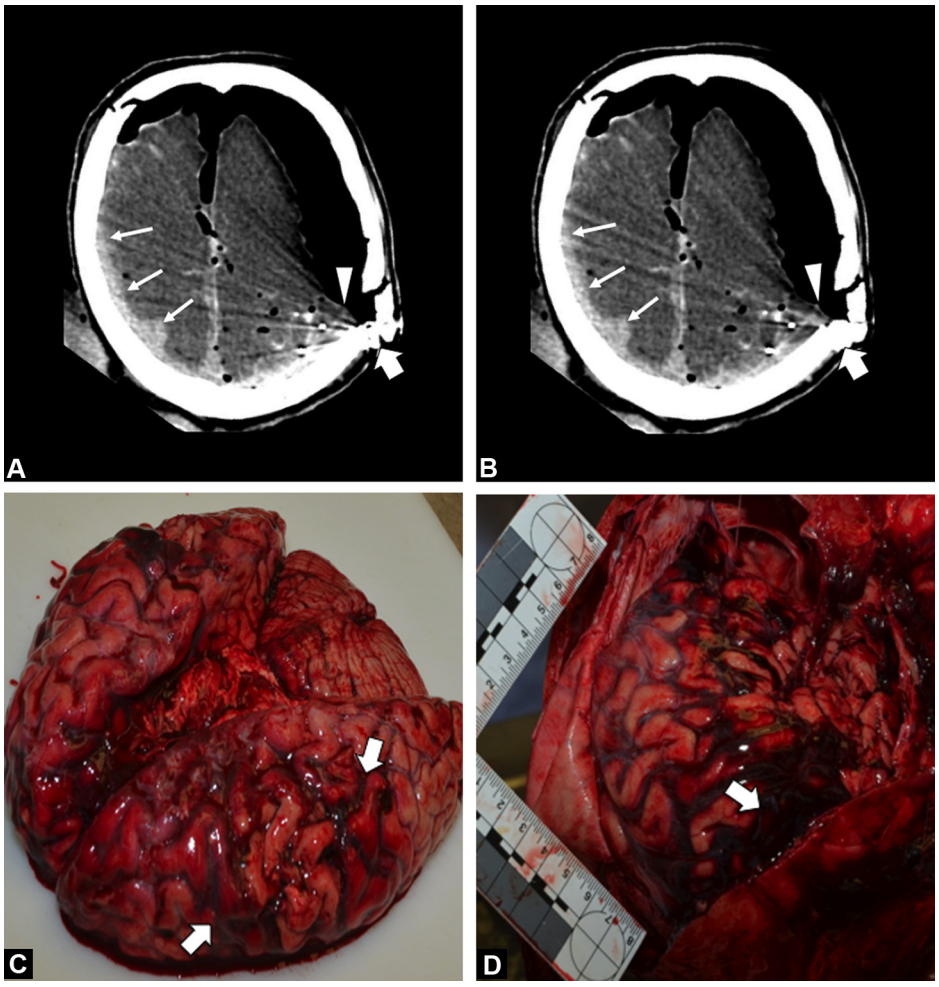

Figure 4. A 78-year old man victim of a head gunshot wound. A and B, CT images in the axial plane obtained with conventional iterative reconstruction and single-energy metal artifact reduction (SEMAR) respectively demonstrate a metallic foreign body (fat arrows). Spontaneous hyperdensity can be seen in both images (thin arrows) and was interpreted as an acute subdural hematoma (ASDH) by two readers. With single-energy metal artifact reduction (B) and a linear image delineating a crescent-shaped fluid collection is seen adjacent to the skull fracture (arrowhead). This image was very difficult to identify with conventional iterative reconstruction (arrowhead in A) and was interpreted as an epidural collection by Reader 1. C and D, Photographs obtained during autopsy confirm diffuse subarachnoid hemorrhage (arrows in C) and right ASDH (arrow in D). The left-sided crescent image seen in B was misinterpreted by the reader and corresponded to an ASDH.

false positive and false negative EAH diagnoses increased with SEMAR compared to conventional IR. This observation could be related to the relative increase in the DZ ratios per fragment and per patient, despite the overall reduction in ATS; thus indicating that despite improved CT image quality, characterizing EAH in subjects with head gunshot wounds with PMCT remains challenging. SEMAR did not influence DZ ratios per fragment compared to conventional IR. These results suggest that SEMAR is more effective in reducing the NIZ compared DZ. Thus, NIZ decreases as it is partially substituted by DZ, increasing the DZ/TA ratio. As the ATS is significantly reduced with SEMAR compared to conventional IR, despite the paradoxical increase in DZ-TA ratio, the end result is an increase in the analyzable cerebral parenchyma area. Although SEMAR can be recommended to evaluate subjects with gunshot head wounds as it improves global CT image quality compared to conventional IR, residual artifacts hindering CT image analysis still remain.

A hemorrhagic cranial lesion of any kind is relevant in forensic investigations because it indicates that the victim was alive at the time of the gunshot. Although the distinction between intra or EAH is of negligible importance in forensic investigation, this information could be useful to evaluate victims of non-lethal head gunshot wounds and patients with therapeutic cranial metallic foreign bodies (e.g., aneurysm coils). Internal ballistics findings are also paramount for head gunshot wound evaluation on PMCT. Although all entry and exit wounds were correctly identified with PMCT, the small number of subjects and lack of standardization in autopsy reports precluded bullet trajectory assessment in this study. Finally, dual-energy applications on PMCT could be used to assess metal fragment composition based on atomic numbers that could determine the ammunition type [38,39].

Several limitations of this study must be acknowledged. First, as a retrospective study with a small number of cadavers, it does not definitely demonstrate the superiority of SEMAR. Furthermore, a single metal artifact reduction algorithm was evaluated. Although other metal artifact reduction algorithms, particularly those using monochromatic imaging, were not tested, previous studies indicate that the performance of SEMAR is slightly superior to these algorithms [40]. Also, the metal composition of the bullets evaluated was unknown, which may influence the effectiveness of SEMAR. Further investigation is warranted to assess the effect of bullet composition on metal artifact reduction. The measurements of NIZ, DZ, and TA with a freehand ROI could lead to small reader induced variations. Finally, only head gunshot wounds were evaluated in this study, and thus further studies are necessary to assess the efficacy of SEMAR on other types of metallic foreign bodies in other anatomic locations.

In conclusion, SEMAR significantly improves CT image quality of PMCT cerebral parenchyma with a significant decrease in NIZ and ATS ratios. This technique leads to increased diagnostic confidence for EAH lesions allowing the identification of all SAH studied. SEMAR led to a slight decrease in interobserver agreement and did not improve the performance of the identification of EAH, which remained poor. Thus, SEMAR can be recommended for the evaluation of head gunshot wounds, but there was no improvement in the diagnostic performance of intracranial hemorrhagic lesions.

Informed consent and patient details

The authors declare that this report does not contain any personal information that could lead to the identification of the subjects.

Funding

This work did not receive any grant from funding agencies in the public, commercial, or not-for-profit sectors.

Author contributions

All authors attest that they meet the current International Committee of Medical Journal Editors (ICMJE) criteria for Authorship.

Douis, Nicolas: Methodology, Formal Analysis, Investigation, validation, Writing — Original Draft, Writing — Review & Editing.

Formery, Anne-Sophie: Investigation.

Hossu, Gabriela: Methodology, Formal Analysis.

Martrille, Laurent: Resources, supervision.

Kolopp, Martin: Methodology, Investigation.

Gondim Teixeira, Pedro Augusto: Methodology, Formal Analysis, Project Administration, Validation, Writing — Original Draft, Writing — Review & Editing.

Blum, Alain: Conceptualization, Methodology, Project Administration, Validation.

Acknowledgments

We are indebted to Bruno Puyssegur, Joris Houde, and Valérie Lamy for their efforts in case selection and CT image reconstruction. We are also grateful for the support of forensic institute personnel.

Disclosure of interest

The authors declare the following financial or personal relationships that could be viewed as influencing the work reported in this paper: two authors involved in this work (P.A.G.T. and A.B.) participate on a non-remunerated research contract with Canon Medical systems for the development and clinical testing of post processing tools for MSK CT. The other authors have no potential conflicts of interest to disclose.

References

[1] Dumousset E, Souffron V, Macri F, BenSalem D, Gorincour G, Dedouit F. Imagerie postmortem en France: état des lieux en 2017. J Radiol Diagn Inter 2017;98:225—35.

[2] Thali MJ, Yen K, Schweitzer W, Vock P, Boesch C, Ozdoba C, et al. Virtopsy, a new imaging horizon in forensic pathology:

virtual autopsy by postmortem multislice computed tomography (MSCT) and magnetic resonance imaging (MRI)-a feasibility study. J Forensic Sci 2003;48:386—403.
[3] Baglivo M, Winklhofer S, Hatch GM, Ampanozi G, Thali MJ, Ruder TD. The rise of forensic and post-mortem radiology: analysis of the literature between the year 2000 and 2011. J Forensic Radiol Imaging 2013;1:3—9.
[4] Thali MJ, Schweitzer W, Yen K, Vock P, Ozdoba C, Spielvogel E, et al. New horizons in forensic radiology: the 60-second digital autopsy-full-body examination of a gunshot victim by multislice computed tomography. Am J Forensic Med Pathol 2003;24:22—7.
[5] Oehmichen M, Meissner C. Routine techniques in forensic neuropathology as demonstrated by gunshot injury to the head. Leg Med Tokyo Jpn 2009;11:S50—3.
[6] Tartaglione T, Filograna L, Roiati S, Guglielmi G, Colosimo C, Bonomo L. Importance of 3D-CT imaging in single-bullet cranioencephalic gunshot wounds. Radiol Med 2012;117:461—70.
[7] Peschel O, Szeimies U, Vollmar C, Kirchhoff S. Postmortem 3-D reconstruction of skull gunshot injuries. Forensic Sci Int 2013;233:45—50.
[8] Blum A, Kolopp M, Teixeira PG, Stroud T, Noirtin P, Coudane H, et al. Synergistic role of newer techniques for forensic and postmortem CT examinations. AJR Am J Roentgenol 2018;211:3—10.
[9] Kolopp M, Blum A, Leupold M-A, Martrille L. Atypical suicide by submachine gun. J Forensic Sci 2018;64:629—33.
[10] Jeffery AJ, Rutty GN, Robinson C, Morgan B. Computed tomography of projectile injuries. Clin Radiol 2008;63:1160—6.
[11] Blum A, Gervaise A, Teixeira P. Iterative reconstruction: why, how and when? Diagn Interv Imaging 2015;96:421—2.
[12] Tuchtan L, Gorincour G, Kolopp M, Massiani P, Léonetti G, Piercecchi-Marti MD, et al. Combined use of postmortem 3D computed tomography reconstructions and 3D-design software for postmortem ballistic analysis. Diagn Interv Imaging 2017;98:809—12.
[13] Garetier M, Deloire L, Dédouit F, Dumousset E, Saccardy C, Ben Salem D. Postmortem computed tomography findings in suicide victims. Diagn Interv Imaging 2017;98:101—12.
[14] Di Maio VJM. An introduction to the classification of gunshot wounds. In: Gunshot wounds: practical aspects of firearms, ballistics, and forensic techniques. 2nd Edition CRC Press; 1998. p. 64—121.
[15] Thali MJ, Viner MD, Brogdon BG. Forensic radiology of gunshot wound, new developments in gunshot injury. In: Brogdon's Forensic Radiology. Second Edition CRC Press; 2011. p. 211—52.
[16] Levy AD, Harcke HT. Gunshot wounds. In: Essentials of Forensic Imaging. CRC Press; 2011. p. 53—95.
[17] Makhlouf F, Scolan V, Ferretti G, Stahl C, Paysant F. Gunshot fatalities: correlation between post-mortem multi-slice computed tomography and autopsy findings: a 30-months retrospective study. Leg Med Tokyo Jpn 2013;15:145—8.
[18] Oehmichen M, Meissner C, König HG, Gehl H-B. Gunshot injuries to the head and brain caused by low-velocity handguns and rifles: a review. Forensic Sci Int 2004;146:111—20.
[19] Verhoff MA, Karger B, Ramsthaler F, Obert M. Investigations on an isolated skull with gunshot wounds using flat-panel CT. Int J Legal Med 2008;122:441—5.
[20] Viel G, Gehl A, Sperhake JP. Intersecting fractures of the skull and gunshot wounds: case report and literature review. Forensic Sci Med Pathol 2009;5:22—7.
[21] Barrett JF, Keat N. Artifacts in CT: recognition and avoidance. Radiographics 2004;24:1679—91.
[22] Boas FE, Fleischmann D. CT artifacts: causes and reduction techniques. Imaging Med 2012;4:229—40.
[23] Sonoda A, Nitta N, Ushio N, Nagatani Y, Okumura N, Otani H, et al. Evaluation of the quality of CT images acquired with the single energy metal artifact reduction (SEMAR) algorithm in patients with hip and dental prostheses and aneurysm embolization coils. Jpn J Radiol 2015;33:710—6.
[24] Yasaka K, Kamiya K, Irie R, Maeda E, Sato J, Ohtomo K. Metal artefact reduction for patients with metallic dental fillings in helical neck computed tomography: comparison of adaptive iterative dose reduction 3D (AIDR 3D), forward-projected model-based iterative reconstruction solution (FIRST) and AIDR 3D with single-energy metal artefact reduction (SEMAR). Dento Maxillo Facial Radiol 2016;45:20160114.
[25] Bier G, Bongers MN, Hempel J-M, Örgel A, Hauser T-K, Ernemann U, et al. Follow-up CT and CT angiography after intracranial aneurysm clipping and coiling-improved image quality by iterative metal artifact reduction. Neuroradiology 2017;59:649—54.
[26] Kidoh M, Utsunomiya D, Ikeda O, Tamura Y, Oda S, Funama Y, et al. Reduction of metallic coil artefacts in computed tomography body imaging: effects of a new single-energy metal artefact reduction algorithm. Eur Radiol 2016;26:1378—86.
[27] Pjontek R, Önenköprülü B, Scholz B, Kyriakou Y, Schubert GA, Nikoubashman O, et al. Metal artifact reduction for flat panel detector intravenous CT angiography in patients with intracranial metallic implants after endovascular and surgical treatment. J Neurointerventional Surg 2016;8:824—9.
[28] Chintalapani G, Chinnadurai P, Srinivasan V, Chen SR, Shaltoni H, Morsi H, et al. Evaluation of C-arm CT metal artifact reduction algorithm during intra-aneurysmal coil embolization: assessment of brain parenchyma, stents and flow-diverters. Eur J Radiol 2016;85:1312—21.
[29] Blum A, Gondim-Teixeira P, Gabiache E, Roche O, Sirveaux F, Olivier P, et al. Developments in imaging methods used in hip arthroplasty: a diagnostic algorithm. Diagn Interv Imaging 2016;97:735—47.
[30] Berger F, Niemann T, Kubik-Huch RA, Richter H, Thali MJ, Gascho D. Retained bullets in the head on computed tomography - Get the most out of iterative metal artifact reduction. Eur J Radiol 2018;103:124—30.
[31] Gondim Teixeira PA, Meyer J-B, Baumann C, Raymond A, Sirveaux F, Coudane H, et al. Total hip prosthesis CT with single-energy projection-based metallic artifact reduction: impact on the visualization of specific periprosthetic soft tissue structures. Skeletal Radiol 2014;43:1237—46.
[32] Chang YB, Xu D, Zamyatin AA.Metal artifact reduction algorithm for single energy and dual energy CT scans. 2012. p. 3426—9 [2012 IEEE Nucl. Sci. Symp. Med. Imaging Conf. Rec. NSSMIC].
[33] Osborn AG, Blaser SI, Salzman KL. Diagnostic Imaging: Brain. Salt Lake City: W B Saunders Co Ltd; 2004.
[34] Blum A, Feldmann L, Bresler F, Jouanny P, Briançon S, Régent D. Value of calculation of the kappa coefficient in the evaluation of an imaging method. J Radiol 1995;76:441—3.
[35] Shiraishi Y, Yamada Y, Tanaka T, Eriguchi T, Nishimura S, Yoshida K, et al. Single-energy metal artifact reduction in postimplant computed tomography for I-125 prostate brachytherapy: impact on seed identification. Brachytherapy 2016;15:768—73.
[36] Pan Y-N, Chen G, Li A-J, Chen Z-Q, Gao X, Huang Y, et al. Reduction of metallic artifacts of the post-treatment Intracranial aneurysms: effects of single energy metal artifact reduction algorithm. Clin Neuroradiol 2017.
[37] Ragusi MAAD, van der Meer RW, Joemai RMS, van Schaik J, van Rijswijk CSP. Evaluation of CT angiography image quality acquired with single-energy metal artifact reduction (SEMAR) algorithm in patients after complex endovascular aortic Repair. Cardiovasc Intervent Radiol 2018;41:323—9.
[38] Gascho D, Zoelch N, Richter H, Buehlmann A, Wyss P, Schaerli S. Identification of bullets based on their metallic components and X-ray attenuation characteristics at different energy levels on CT. AJR Am J Roentgenol 2019;213:1—9.

[39] Winklhofer S, Stolzmann P, Meier A, Schweitzer W, Morsbach F, Flach P, et al. Added value of dual-energy computed tomography versus single-energy computed tomography in assessing ferromagnetic properties of ballistic projectiles: implications for magnetic resonance imaging of gunshot victims. Invest Radiol 2014;49:431—7.

[40] Bolstad K, Flatabø S, Aadnevik D, Dalehaug I, Vetti N. Metal artifact reduction in CT, a phantom study: subjective and objective evaluation of four commercial metal artifact reduction algorithms when used on three different orthopedic metal implants. Acta Radiol 1987 2018;59:1110—8.